Mixed formulation and finite element treatment of the mass-conserving cavitation model

Jakub Lengiewicz[a], Michał Wichrowski[b], Stanisław Stupkiewicz[a,*]

[a]*Institute of Fundamental Technological Research (IPPT), Polish Academy of Sciences, Pawińskiego 5B, 02–106 Warsaw, Poland*
[b]*Warsaw University of Technology, Institute of Aeronautics and Applied Mechanics, Nowowiejska 24, 00-665 Warsaw, Poland*

Abstract

A mixed formulation of the mass-conserving cavitation model is developed. The cavitation problem is formulated in terms of the hydrodynamic pressure and a complementary variable representing the void fraction in the cavitation zone. Weak form of the mass-balance equation is consistently derived, and it exhibits subtle differences with respect to the available formulations. Finite element treatment preserves the two-field formulation, and a semi-smooth Newton method is applied to solve the resulting discretized equations. A monolithic Newton-based scheme is also applied to solve the fully coupled elastohydrodynamic lubrication problem in the soft-EHL regime. Numerical examples illustrate the performance of the computational scheme.

Keywords: lubrication, cavitation, Reynolds equation, soft-EHL problem

1. Introduction

Adequate treatment of cavitation constitutes an important part of computational modelling of hydrodynamic lubrication problems. Position of the cavitation boundary is not known a priori which makes the corresponding free-boundary problem computationally demanding, particularly when severe nonlinearities due to the elastohydrodynamic coupling are additionally considered.

---

*Corresponding author. Email address: sstupkie@ippt.pan.pl

Early models of cavitation did not guarantee mass conservation. This has been circumvented once appropriate boundary conditions have been formulated on the cavitation boundary. These are attributed to Jakobsen and Floberg [1] and Olsson [2], and the corresponding model is often referred to as the JFO theory. Elrod and Adams [3, 4] proposed a successful computational algorithm that implements the JFO mass-conserving cavitation model and is based on the finite difference method. Since then, several numerical algorithms have been developed, in which the essential features of the JFO model are preserved. The corresponding representative developments include Refs. [5–7] in the context of the finite difference method and Refs. [8–12] in the context of the finite element method. Other related approaches can be found, for instance, in [13, 14].

The general structure of the mass-conserving model of cavitation in hydrodynamic lubrication problems seems now commonly accepted, and the various approaches mentioned above differ in the details of formulation and computational treatment. It should be reminded here that the JFO model of cavitation is a simplification of a complex physical phenomenon, and more refined models may be necessary in specific situations, see the review [15]. For instance, a two-phase flow approach is adopted in [16] thus providing a refined description of the interaction between liquid and gas and of the corresponding changes in lubricant properties, and a cavitation model accounting for bubble dynamics and surface tension effects is proposed in [17]. In a recent paper, Bayada and Chupin [18] present an extended review of various types of cavitation models and subsequently develop a vaporous cavitation model starting from the compressible Navier-Stokes equation.

The free boundary problems of lubrication and cavitation are often formulated by referring to complementarity of some of the involved variables. This has been recognized long time ago [19–21]; however, those early models do not guarantee mass-conservation. Recently, Giacopini et al. [22] have formulated the mass-conserving cavitation model as a linear complementarity problem (LCP) which they solve using a suitable pivoting algorithm. This LCP-based formulation is extended in [23] to nonlinear problems involving lubricant compressibility, piezoviscous and non-Newtonian effects.

Complementarity of the hydrodynamic pressure and lubricant density (or the like) is also exploited in other mass-conserving formulations, cf. [8, 9, 12]. A typical example is the formulation of Hajjam and Bonenau [12] in which a single variable is introduced from which the fields of the pressure and the complementary variable are uniquely reconstructed. That approach is

opposed to the Elrod–Adams algorithm [3, 4] in which fluid compressibility is assumed in the full-film region so that pressure and density are related by a constitutive relationship, and the problem can be formulated in terms of a single variable.

The long-term motivation for the present work is to develop a consistent formulation and the corresponding computational scheme for the analysis of elastohydrodynamic lubrication (EHL) problems in the so-called soft-EHL regime. In the soft-EHL (or elastic-isoviscous) regime, the pressure is relatively low, so that the related increase of lubricant viscosity is not significant, but one or both contacting bodies are relatively soft so that elastic deflections are significant. The problems of interest include elastomeric seals, various biotribological systems, and others. Problems of this kind typically involve finite deformations of the contacting bodies. The linear elasticity framework, as usually adopted in the EHL theory, is then not fully adequate, though often used as an approximation, e.g., [24]. A fully consistent formulation should thus include finite deformation effects, and an adequate computational method must be used to solve the corresponding finite deformation subproblem. Furthermore, in view of finite deformations, the lubrication and cavitation subproblem must be solved on the lubricated contact boundary which undergoes finite configuration changes. A fully coupled formulation suitable for this class of problems has been recently developed in [25, 26]. The formulation employs the finite element method to solve both subproblems in a monolithic manner. In this work, that formulation is extended to three-dimensional problems (the lubrication subproblem being thus two-dimensional), and the mass-conserving cavitation model is used instead of the penalty formulation adopted in [25, 26].

To this end, a mixed formulation of the mass-conserving cavitation model has been developed which is more flexible than the available single-field formulations. In the present two-field mixed formulation, the governing equations of the lubrication and cavitation subproblem are expressed in terms of the hydrodynamic pressure and an additional complementary variable that is used to enforce the inequality constraint imposed on the pressure due to cavitation. The complementary variable has a physical meaning of void fraction in the cavitated region. Compared to the single-field formulations, e.g. [12], introduction of the additional variable gives more flexibility in constructing finite-element discretization schemes while the two are fully equivalent in the continuum setting (hence the name 'mixed' formulation, cf. [27]).

The adopted continuum formulation derives from the classical JFO the-

3

ory. The weak formulation which constitutes the basis of the finite element implementation is then consistently derived. Extra terms appear in the resulting weak form that are not present in the formulations available in the literature. One of those terms involves integration over the cavitation boundary. This term vanishes once a continuous finite element approximation is introduced. The second difference is due to the complementary variable present in the Poiseuille term which makes the lubrication and cavitation subproblem a nonlinear complementarity problem, as opposed to the linear complementarity formulation of [22]. The corresponding effects are investigated in the numerical examples and are found to have a minor effect on the accuracy of the finite-element scheme.

The conditions under which the proposed formulation is equivalent to the single-field formulation of Hajjam and Bonneau [12] are also discussed. In particular, we point out the situations in which the present two-field formulation is beneficial, despite it involves additional unknowns as compared to the single-field formulation of [12].

The final numerical example of this paper presents an application of the proposed mixed formulation of the mass-conserving cavitation model to a soft-EHL problem that includes advanced features such as finite deformations, loading due to shear stresses in the lubricant, and a fully coupled, monolithic solution scheme.

2. Mass-conserving cavitation model

2.1. Governing equations

The hydrodynamic lubrication theory is concerned with modelling of fluid flow in a thin film between two surfaces in relative motion. Denote by Ω the two-dimensional domain of interest which is split into the full-film region Ω_f and the cavitated region Ω_c with the interface separating the two regions, the cavitation boundary, denoted by Σ, cf. Fig. 1.

In steady-state conditions, the mass-balance equation can be written as

$$\nabla \cdot (\varrho \boldsymbol{q}) = 0 \quad \text{in } \Omega, \tag{1}$$

where $\boldsymbol{q}$ is the volumetric flux and ϱ the density.

In the full-film region Ω_f, the flow is governed by the classical Reynolds equation according to which the flux is given by

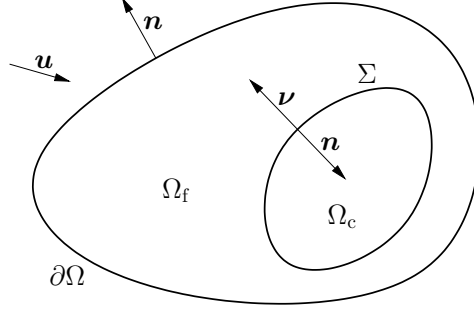$$\boldsymbol{q} = \boldsymbol{u}h - \frac{h^3}{12\eta} \nabla p \quad \text{in } \Omega_f, \tag{2}$$

4

Figure 1: Notation.

where p is the pressure, h the film thickness, $\boldsymbol{u} = \frac{1}{2}(\boldsymbol{u}_1 + \boldsymbol{u}_2)$ the average velocity of the surfaces (also called the entrainment speed), and η the lubricant viscosity.

The commonly adopted model of cavitation assumes that cavitation occurs whenever the pressure drops to the cavitation pressure p_{cav}, and the pressure is constant and equal to the cavitation pressure $p = p_{\text{cav}}$ in the cavitated region, so that

$$p \geq p_{\text{cav}} \quad \text{in } \Omega \qquad \text{and} \qquad p = p_{\text{cav}} \quad \text{in } \Omega_{\text{c}}. \tag{3}$$

The cavitating fluid is a mixture of liquid, vapor, and gas. As a result, its density ϱ is lower than the density ϱ_0 of the intact fluid, the latter is assumed constant, i.e., the fluid is assumed incompressible in the full-film region Ω_{f},

$$\varrho \leq \varrho_0 \quad \text{in } \Omega \qquad \text{and} \qquad \varrho = \varrho_0 \quad \text{in } \Omega_{\text{f}}. \tag{4}$$

It is assumed that the flux in the cavitated region Ω_{c} is only due to the Couette-like flow, thus

$$\boldsymbol{q} = \boldsymbol{u}h \quad \text{in } \Omega_{\text{c}}. \tag{5}$$

The mass-balance equation (1) with the flux defined by (2) and (5) must be accompanied by the continuity condition that enforces the mass balance on the cavitation boundary Σ,

$$(\varrho^+ \boldsymbol{q}^+ - \varrho^- \boldsymbol{q}^-) \cdot \boldsymbol{\nu} = 0 \quad \text{on } \Sigma, \tag{6}$$

where $\boldsymbol{\nu}$ is the unit vector normal to Σ and oriented outwards from Ω_{c}, and the superscripts $+$ and $-$ denote the limit values of the corresponding quantities as Σ is approached from the full-film and cavitated side, respectively.

5

Finally, the Dirichlet boundary conditions are assumed on the whole boundary of the domain Ω,

$$p = p^* \quad \text{on } \partial\Omega, \tag{7}$$

where $p^* \geq p_{\text{cav}}$ is a given prescribed pressure.

Remark 1. The mass-flux continuity condition (6) with the cavitation conditions (3) and (4) imply the well-known boundary conditions of the JFO theory. On the film rupture boundary, where $\boldsymbol{u} \cdot \boldsymbol{\nu} < 0$, the density ϱ is continuous so that we have

$$p = p_{\text{cav}} \quad \text{and} \quad (\nabla p)^+ \cdot \boldsymbol{\nu} = 0. \tag{8}$$

On the reformation boundary, where $\boldsymbol{u} \cdot \boldsymbol{\nu} > 0$, the density ϱ suffers discontinuity which, in view of condition (6), implies discontinuity of the pressure gradient, thus

$$p = p_{\text{cav}} \quad \text{and} \quad \frac{\varrho^+ h^3}{12\eta}(\nabla p)^+ \cdot \boldsymbol{\nu} = (\varrho^+ - \varrho^-)h\boldsymbol{u} \cdot \boldsymbol{\nu}. \tag{9}$$

The subsequent developments are based on the general continuity condition (6), and the film rupture and reformation boundaries need not be considered separately.

Remark 2. Equations (1), (2) and (5) are equivalent to the so-called p–θ formulation of Elrod and Adams [3]. In fact, considering that pressure gradient is equal to zero in the cavitation zone (since $p = p_{\text{cav}}$), cf. Eq. $(3)_2$, equations (1), (2) and (5) can be written jointly as

$$\nabla \cdot \left(\bar{\varrho}\boldsymbol{u}h - \frac{\bar{\varrho}h^3}{12\eta}\nabla p \right) = 0 \quad \text{in } \Omega, \tag{10}$$

where the relative density $\bar{\varrho} = \varrho/\varrho_0$ corresponds to the θ variable of the p–θ formulation. Note, however, that Eq. (10) does not imply that the continuity condition (6) is satisfied on the cavitation boundary Σ.

2.2. Governing equations in weak form

In this section, the weak form of the governing equations is derived which is the basis of the subsequent finite-element formulation of the lubrication and cavitation problem. Derivation of the weak form requires some attention because some of the quantities involved are expected to be discontinuous. Specifically, as it is well known, the density ρ and the flux $\boldsymbol{q}$ suffer discontinuity at the part of Σ at which reformation of full-film lubrication occurs. At the same time, the pressure p is continuous in Ω, though its gradient is not continuous at the reformation boundary.

The weak form of the mass-balance equation is obtained in a standard manner by multiplying Eq. (1) by a continuous test function δp and integrating over the domain Ω,

$$\int_{\Omega} \delta p \, \nabla \cdot (\varrho \boldsymbol{q}) \, \mathrm{d}\Omega = 0. \tag{11}$$

It is reminded that, following a standard argument, Eq. (11) must hold for all test functions δp. Also, in view of the boundary condition (7), the test function δp is assumed to vanish on the boundary $\partial \Omega$,

$$\delta p = 0 \quad \text{on } \partial \Omega. \tag{12}$$

In the next step, Eq. (11) is integrated by parts. Considering that the flux $\boldsymbol{q}$ comprises the Poiseuille (pressure-gradient) term and the Couette (advective) term, integration by parts can be applied either to both terms or only to the Poiseuille term. The latter option is followed in this work due to the specific upwind scheme used in the finite-element implementation. For completeness, the former option is commented in Remark 3 below.

Detailed derivation of the weak form is presented in Appendix A. In brief, the integral over Ω in Eq. (11) is split into two parts corresponding to Ω_{f} and Ω_{c}, the pressure-gradient term is integrated by parts within Ω_{f}, and condition (6) of mass-flux balance at the cavitation boundary Σ is used. As a result, the following weak form of the mass-balance equation in obtained

$$\int_{\Omega} \left[\nabla \delta p \cdot \left(\frac{\bar{\varrho} h^3}{12\eta} \nabla p \right) + \delta p \, \nabla \cdot (\bar{\varrho} \boldsymbol{u} h) \right] \mathrm{d}\Omega + \int_{\Sigma} \delta p (\bar{\varrho}^+ - \bar{\varrho}^-) h \boldsymbol{u} \cdot \boldsymbol{\nu} \, \mathrm{d}\Gamma = 0, \tag{13}$$

where $\bar{\varrho} = \varrho / \varrho_0$ is the relative density which corresponds to the θ variable of the so-called p–θ formulation of Elrod and Adams [3, 4].

The last term in the weak form (13) is related to discontinuity of $\bar{\varrho}$ and involves integration over the cavitation boundary Σ, which would be an undesired feature from the point of view of computational treatment. However, this term vanishes once a *continuous* finite element approximation is introduced, see Section 3.1. Note that this term is missing, for instance, in [12, 22, 23], though this does not affect the corresponding finite element schemes in view of the continuous finite element approximation used.

The two independent variables involved in the weak form (13), namely the pressure p and the density $\bar{\varrho}$, must satisfy the inequality conditions (3) and (4) which are compactly written in the form of the following complementarity conditions

$$p - p_{\mathrm{cav}} \geq 0, \qquad \bar{\varrho} - 1 \leq 0, \qquad (p - p_{\mathrm{cav}})(\bar{\varrho} - 1) = 0, \qquad (14)$$

where the last equation states that the two inequalities are complementary, i.e., at least one of them always holds as an equality.

Equations (13) and (14) with the boundary condition (7) fully define the cavitation problem at hand. In particular, the flux continuity condition (6) need not be enforced separately because it is already included in the weak form (13).

Remark 3. An alternative weak form of the mass-balance equation (1) can be obtained by integrating by parts both the Poiseuille term and the Couette term. Following the procedure outlined in Appendix A and using the flux continuity conditions (6), the following weak form is then obtained

$$\int_{\Omega} \nabla \delta p \cdot \left(\frac{\bar{\varrho} h^3}{12 \eta} \nabla p - \bar{\varrho} \boldsymbol{u} h \right) \mathrm{d}\Omega = 0, \qquad (15)$$

in which integration over the cavitation boundary Σ is avoided. This form is used, for instance, in [8, 28]. However, it is less suitable for the finite element treatment. Specifically, it is not compatible with the upwind scheme that has been applied to stabilize the advection equation in the cavitated region, see Section 3.1. The upwind scheme (23) would not be effective here because the upwind correction modifies the test function, while only the gradient of the test function appears in the weak form (15).

2.3. Mixed formulation of the mass-conserving cavitation model

Let us introduce a variable $\lambda = 1 - \bar{\varrho} \leq 1$ that is interpreted as the void fraction in the cavitated region. Furthermore, let us assume that the cavitation pressure is equal to zero, $p_{\mathrm{cav}} = 0$, which is equivalent to introducing a shifted pressure variable $p' = p - p_{\mathrm{cav}} \geq 0$. The governing equations (13) and (14) take then the following form:

$$\int_{\Omega} \left[\nabla \delta p \cdot \left(\frac{(1-\lambda)h^3}{12\eta} \nabla p \right) + \delta p \, \nabla \cdot [(1-\lambda)\boldsymbol{u}h] \right] \mathrm{d}\Omega$$

$$- \int_{\Sigma} \delta p \, (\lambda^+ - \lambda^-) h \boldsymbol{u} \cdot \boldsymbol{\nu} \, \mathrm{d}\Gamma \;\; = \;\; 0, \qquad (16)$$

$$p \geq 0, \quad \lambda \geq 0, \quad p\lambda = 0 \quad \text{in } \Omega. \qquad (17)$$

The main idea of the proposed mixed formulation is to treat the variable λ in Eqs. (16)–(17) as an independent variable and to enforce the complementarity conditions (17) using a constraint function $C(p, \lambda)$,

$$C(p, \lambda) = 0 \quad \text{in } \Omega, \qquad (18)$$

where

$$C(p, \lambda) = \lambda - \max(0, \lambda - \epsilon p), \qquad (19)$$

for $\epsilon > 0$. It can be easily checked that the complementarity conditions (17) are satisfied for each pair (p, λ) such that $C(p, \lambda) = 0$. We note that the constraint function $C(p, \lambda)$ is continuous, but it is non-smooth along the line $\lambda - \epsilon p = 0$. The value of parameter ϵ does not influence the solution of the problem, nor the convergence of the adopted iterative scheme, see Section 3.1.

Equation (18) enforces complementarity of p and λ locally at each point in Ω. The integral form of the complementarity condition (18) is introduced by multiplying it by a test function $\delta\lambda$ and integrating over Ω, so that the following weak form is obtained

$$\int_{\Omega} \delta\lambda \, C(p, \lambda) \, \mathrm{d}\Omega = 0, \qquad (20)$$

which holds for all test functions $\delta\lambda$.

The way in which the complementarity conditions (17) are enforced in Eq. (18) using the constraint function $C(p, \lambda)$ is similar to the treatment of inequality constraints in the augmented Lagrangian method [29] and in the primal-dual active set strategy [30]. Both approaches lead to highly efficient algorithms that have been successfully applied, for instance, in computational contact mechanics [31, 32].

3. Finite element treatment

The starting point for the finite element treatment of the lubrication and cavitation problem are the weak forms (16) and (20) which express the Reynolds equation jointly with the mass-conserving cavitation model. Finite element treatment of the corresponding steady-state rigid-isoviscous lubrication problem is presented in Section 3.1. In Section 3.2, we show that the present formulation can be transformed to the linear complementarity formulation of [22] by neglecting the nonlinear term $(1 - \lambda)$ in the Poiseuille term. Finally, application of the present cavitation model in a fully coupled soft-EHL problem is discussed in Section 3.3. Extension of the present formulation to transient hydrodynamic lubrication problems is briefly introduced in Appendix B, and a single-field formulation is discussed in Appendix C.

The finite element implementation and the computations reported in this work have been carried out using the *AceGen/AceFEM* system [33]. For brevity, the standard technical details are omitted below.

3.1. Finite element discretization

Finite element approximation of the unknown fields p and λ and their variations (test functions) is introduced in a standard manner,

$$p^h = \sum_i N_i p_i, \quad \lambda^h = \sum_i N_i^\lambda \lambda_i, \quad \delta p^h = \sum_i N_i \delta p_i, \quad \delta \lambda^h = \sum_i N_i^\lambda \delta \lambda_i, \tag{21}$$

where N_i and N_i^λ are continuous shape (basis) functions, and p_i and λ_i are the corresponding nodal quantities. Although the solution of the cavitation problem is known to exhibit discontinuity of λ at the reformation boundary, an approximate solution is here sought in the class of continuous functions. The expected jump in λ will thus be approximated by a continuous function with a high gradient at the reformation boundary.

In view of continuity of λ^h, the last term in the weak form (16) vanishes, so that the discretized weak form reads

$$\int_{\Omega^h} \left[\nabla \delta p^h \cdot \left(\frac{(1 - \lambda^h) h^3}{12\eta} \nabla p^h \right) + \delta p^h \nabla \cdot [(1 - \lambda^h) \boldsymbol{u} h] \right] \mathrm{d}\Omega = 0. \tag{22}$$

The problem that is actually solved in the cavitated region is a pure advection problem for λ. The product $\boldsymbol{u}h$ plays the role of advection velocity, and the corresponding Péclet number is infinite, as there is no associated diffusion. It is well known that standard (Galerkin) finite element formulations

10

are not suitable for problems of this kind. A possible solution is to apply an upwind scheme to the advection term in Eq. (22). The approach adopted in this work derives from the streamline diffusion method [34] that is closely related to the streamline upwind/Petrov-Galerkin (SUPG) method [35, 36]. The test function δp is replaced by a discontinuous one, $\delta \tilde{p}$, that includes an upwind correction,

$$\delta \tilde{p} = \delta p + \kappa \hat{\boldsymbol{u}} \cdot \nabla \delta p, \qquad \kappa = h_e/2, \tag{23}$$

where $\hat{\boldsymbol{u}} = \boldsymbol{u}/|\boldsymbol{u}|$ and h_e denotes the element size (not to be mistaken with the film thickness h). The adopted value of the upwind parameter $\kappa = h_e/2$ is a special case of the optimal upwind scheme [35] corresponding to pure advection. It has been checked that adopting a smaller value of $\kappa = h_e/\sqrt{15}$, as suggested in [35] specifically for the case of pure advection, does improve accuracy for coarse meshes, but the corresponding scheme becomes unstable for finer meshes. A similar upwind scheme has been recently used in [23].

The discretized problem is thus finally governed by the following weak forms

$$\int_{\Omega^h} \left[\nabla \delta p^h \cdot \left(\frac{(1-\lambda^h)h^3}{12\eta} \nabla p^h \right) + \delta p^h \, \nabla \cdot (\boldsymbol{u}h) - \delta \tilde{p}^h \, \nabla \cdot (\lambda^h \boldsymbol{u}h) \right] \mathrm{d}\Omega = 0, \tag{24}$$

$$\int_{\Omega^h} \delta \lambda^h \, C(p^h, \lambda^h) \, \mathrm{d}\Omega = 0, \tag{25}$$

with boundary conditions (7).

As the last step, the integrals in Eqs. (24) and (25) are evaluated by numerical integration. Following the standard approach, integration over element domains Ω_e is approximated by summation over the quadrature points, thus

$$\int_{\Omega^h} \phi(\boldsymbol{x}) \mathrm{d}\Omega = \sum_e \int_{\Omega_e} \phi(\boldsymbol{x}) \mathrm{d}\Omega \approx \sum_e \sum_g \omega_g j(\boldsymbol{\xi}_g) \phi(\boldsymbol{x}(\boldsymbol{\xi}_g)), \tag{26}$$

where $\phi(\boldsymbol{x})$ denotes a generic function, $\boldsymbol{\xi}$ are the coordinates of a local parametrization of Ω_e, j is the Jacobian of the corresponding transformation, and ω_g is the weight of a quadrature point $\boldsymbol{\xi}_g$.

In the present implementation, four-node quadrilateral elements are used, and the same bilinear shape functions are used to interpolate p and λ. This is combined with the standard Gaussian quadrature of the mass-balance equation (24) with 2×2 integration points (in one-dimensional problems, linear

elements with 2 integration points are used). Numerical tests (not reported in this work) have shown that the Gaussian quadrature is more accurate in reproducing the pressure field than the nodal (Lobatto) quadrature. However, the nodal quadrature has some advantages in two-dimensional problems, see Section 4.3.

In case of the complementarity equation (25), stable schemes have been obtained only for the nodal quadrature. The complementarity conditions are thus enforced at the nodes of the finite element mesh. Nodal enforcement of the complementarity conditions is directly assumed, for instance, in [12, 22, 23].

Upon the finite element discretization, as introduced above, Eqs. (24) and (25) are written as

$$(\delta \mathbf{p})^{\mathrm{T}} \mathbf{r}_p(\mathbf{p}, \boldsymbol{\lambda}) = 0, \qquad (\delta \boldsymbol{\lambda})^{\mathrm{T}} \mathbf{r}_\lambda(\mathbf{p}, \boldsymbol{\lambda}) = 0, \qquad (27)$$

where $\mathbf{p}$ and $\boldsymbol{\lambda}$ are the vectors of unknown nodal pressures p_i and void fractions λ_i, respectively, and $\mathbf{r}_p$ and $\mathbf{r}_\lambda$ are the corresponding nodal residual vectors. Equations (27) hold for arbitrary $\delta \mathbf{p}$ and $\delta \boldsymbol{\lambda}$, so that the following system of algebraic equations is obtained,

$$\mathbf{r}(\mathbf{u}) = \mathbf{0}, \qquad \mathbf{r} = \{\mathbf{r}_p, \mathbf{r}_\lambda\}, \qquad \mathbf{u} = \{\mathbf{p}, \boldsymbol{\lambda}\}. \qquad (28)$$

An iterative scheme is applied to solve Eq. (28),

$$\mathbf{u}^{k+1} = \mathbf{u}^k + \Delta \mathbf{u}^k, \qquad \Delta \mathbf{u}^k = -\left(\frac{\partial \mathbf{r}}{\partial \mathbf{u}}\right)^{-1} \mathbf{r}(\mathbf{u}^k), \qquad (29)$$

which can be interpreted as a semi-smooth Newton method, as the constraint function $C(p, \lambda)$ is non-smooth at $\lambda - \epsilon p = 0$. The iterative scheme is typically initiated by setting $\mathbf{u}^0 = \mathbf{0}$. Alternatively, a solution of the previous step is used as a starting point at the current step when an incremental problem is considered. The latter option is followed in the transient lubrication problem of Section 4.4 and in the soft-EHL problem of Section 4.5. Numerical examples studied in Sections 4.1–4.4 indicate that the above iterative scheme performs satisfactorily for both steady-state and transient lubrication problems.

Remark 4. The value of parameter ϵ in Eq. (19) does not influence the convergence of the iterative scheme (29). As the nodal quadrature is applied

12

to the weak form (25), the complementarity conditions (17) are automatically satisfied at all nodes after each Newton iteration, see also the first paragraph in Appendix C. Thus the state of each node (full film or cavitation) is determined regardless of the value of ϵ, and $\epsilon = 1$ can simply be used (with a proper dimension to maintain consistency). The value of ϵ might influence the convergence if, for instance, a line search technique was applied.

3.2. Linear complementarity problem

In the continuum setting, the complementarity conditions (17) imply that the pressure gradient is equal to zero in the cavitation region where $\lambda > 0$. Accordingly, the term $(1 - \lambda)\nabla p$ in Eq. (16) could be replaced by ∇p alone since in the full-film region we have $\lambda = 0$ and $\nabla p \neq \mathbf{0}$, while in the cavitated region we have $\lambda > 0$ and $\nabla p = \mathbf{0}$. Then, proceeding as described in the previous subsection, the following discrete weak form is obtained

$$\int_{\Omega^h} \left[\nabla \delta p^h \cdot \left(\frac{h^3}{12\eta} \nabla p^h \right) + \delta p^h \nabla \cdot (\boldsymbol{u}h) - \delta \tilde{p}^h \nabla \cdot (\lambda^h \boldsymbol{u}h) \right] \mathrm{d}\Omega = 0, \quad (30)$$

instead of that in Eq. (24), where the only difference is that the term $(1 - \lambda^h)$ is not present in the Poiseuille term in Eq. (30).

It has been noted by Giacopini et al. [22], that Eq. (30) defines a linear complementarity problem (LCP). Indeed, the residual vector $\mathbf{r}_p^{\mathrm{lin}}(\mathbf{p}, \boldsymbol{\lambda})$ corresponding to the weak form (30) is now linear in $\mathbf{p}$ and $\boldsymbol{\lambda}$ so that the mass-balance equation can be written as

$$\mathbf{r}_p^{\mathrm{lin}}(\mathbf{p}, \boldsymbol{\lambda}) = \mathbf{A}\mathbf{p} + \mathbf{B}\boldsymbol{\lambda} + \mathbf{c} = \mathbf{0}, \quad (31)$$

where $\mathbf{A}$ and $\mathbf{B}$ are constant matrices, and $\mathbf{c}$ is a constant vector. By introducing the same interpolation for p and λ and enforcing the complementarity conditions at the nodes,

$$p_i \geq 0, \quad \lambda_i \geq 0, \quad p_i \lambda_i = 0, \quad (32)$$

the cavitation problem has exactly the structure of a linear complementarity problem, and it can be solved using any of the methods available for this class of problems.

We note that the LCP-based formulation of the cavitation problem is only applicable in the rigid-isoviscous lubrication regime. In fact, the complementarity problem is no longer linear when elastohydrodynamic or piezoviscous

couplings occur, i.e., when, respectively, the film thickness h or the viscosity η depend on the pressure p. As an extension of the LCP formulation of [22], an iterative scheme applicable to nonlinear problems including compressibility, piezoviscous and non-Newtonian effects has been developed in [23].

Secondly, we note that the condition $\lambda \nabla p = \mathbf{0}$, which implies the weak form (30) instead of (22), is satisfied only in the continuum setting. Once the finite element approximation (21) is introduced, complementarity of p^h and λ^h cannot be enforced in the whole domain Ω^h. Specifically, in the present formulation, the condition $\lambda^h \nabla p^h = 0$ is not satisfied within the elements belonging to the cavitation boundary.[1] The nonlinear formulation (22) involving λ^h in the Poiseuille term seems thus more consistent and is expected to be more accurate than the linear one in Eq. (30). This is confirmed by the numerical examples in Section 4, though the effect is small or even negligible. As also illustrated in Section 4, the nonlinear formulation may lead to numerical problems such as lack of convergence or convergence to a non-physical solution. For these reasons, it is concluded that the linear formulation (30) appears preferable in practical computations.

3.3. Fully coupled soft-EHL problem

The cavitation model, discussed so far in the context of rigid-isoviscous lubrication regime, can be readily applied to modelling of elastohydrodynamic lubrication problems. Specifically, our interest is in soft-EHL problems involving finite deformations of the solid. The corresponding formulation has been developed in [25, 26] and is very briefly outlined in this section.

Lubricated contact of a hyperelastic solid is considered with a full account for finite configuration changes. The counter surface is assumed to be a rigid plane. In the solid part, which is rather standard, the hyperelastic body is discretized using the finite element method so that the geometry, finite deformations and nonlinear material behaviour can be adequately represented (here, eight-node elements employing the F-bar formulation [37] are used to avoid volumetric locking effects). The loading, i.e. the hydrodynamic pressure and the shear stress in the lubricant, is applied on the lubricated boundary as a surface traction. Note that the friction forces are usually neglected in EHL models, although they may have a significant impact on the solution, cf. [25].

---

[1]The cavitation boundary is formed by those elements in which the status of all the nodes (full-film lubrication or cavitation) is not identical.

The Reynolds equation, including the mass-conserving cavitation model, is formulated and solved in the current (deformed) configuration of the solid. The deformed mesh of the lubricated boundary of the solid is projected on the counter surface (which is straightforward in the case of a rigid plane), and this projected mesh constitutes the actual finite element mesh on which the Reynolds equation is solved. The weak form of the mass-balance equation (30) is used without any modification, and so is the complementarity condition (25).

The resulting nonlinear equations are solved monolithically for all global unknowns using the Newton method. The unknowns include the nodal values of the displacement field of the solid as well as the pressure p and the complementary variable λ on the lubricated boundary of the solid. Additionally, since mesh refinement is used, the unknowns include also Lagrange multipliers prescribing the variables at the so-called hanging nodes. The tangent matrix needed in the Newton method is obtained by full linearization of the nonlinear finite element equations. This is achieved using the automatic differentiation technique available in the *AceGen/AceFEM* system [33]. As the constraint function $C(p, \lambda)$ in Eq. (25) is nonsmooth, the iterative scheme is in fact a semi-smooth Newton method.

The linearization includes the usual elastohydrodynamic coupling. The local film thickness h depends on the actual distance between the two surfaces, so it depends on the displacements of the solid. At the same time, deformation of the solid depends on the pressure p which is governed by the lubrication subproblem.

However, there is an additional coupling which is due to the finite deformation effects. As mentioned above, the Reynolds equation is solved in the deformed configuration. The nodal positions depend thus on the displacements, and this dependence must also be accounted for when linearizing the finite element equations.

The soft-EHL problem, such as that studied in Section 4.5, is highly nonlinear as it involves finite deformations, elastohydrodynamic coupling and nonsmooth behaviour introduced by the cavitation model. Accordingly, a kind of path-following technique is used to obtain the solution corresponding to a prescribed loading. Specifically, a sequence of steady-state EHL problems is solved for incrementally increasing loading, and, at each step, the iterative Newton method is applied with the solution from the previous step used as the initial guess. We remind that the problem is solved monolithically for all unknowns. Once the prescribed loading is achieved, the entrainment

speed is varied so that the complete response corresponding to a fixed loading is computed in an efficient manner.

Compared to [25, 26], the present formulation differs in the way the cavitation is treated: the penalty formulation was used in [25, 26], while here the mass-conserving cavitation model is used. Furthermore, the formulation has been extended to three-dimensional problems, but this is merely an implementation issue. A related numerical example is presented in Section 4.5.

4. Numerical examples

4.1. Sinusoidal bearing profile

As the first example, consider a one-dimensional problem of steady-state hydrodynamic lubrication in a sinusoidal bearing with the parameters of the problem taken from [22]. The film thickness is defined as

$$h(x) = h_{\mathrm{av}} - \Delta h \cos(2\pi x/l), \qquad x \in (-l/2, l/2), \tag{33}$$

where $h_{\mathrm{av}} = 0.02$ mm, $\Delta h = 0.005$ mm, and $l = 125$ mm. The lubricant viscosity is $\eta = 0.015$ Pa s, the entrainment speed is $u = 2$ m/s, and the boundary conditions are prescribed as $p(\pm l/2) = 1$ MPa.

A reference analytical solution to this problem has been used in the study of the accuracy of the finite element scheme. The analytical solution has been obtained by integrating the Reynolds equation symbolically using *Mathematica*. The position of the film-rupture boundary has then been obtained numerically by requiring that the pressure and its derivative are equal to zero at this boundary. Finally, the position of the reformation boundary has been obtained numerically by requiring that the pressure is equal to zero at this boundary and that the mass flux is preserved in the full film region. The void fraction λ is obtained from the mass-conservation equation in the cavitated region. The analytical solution exhibits two essential features: the pressure gradient is equal to zero at the film-rupture boundary, and both the pressure gradient and the void fraction λ are discontinuous at the reformation boundary. The respective code in *Mathematica* is provided as a supplementary material accompanying this paper.[2]

The analytical solution and two sample FE solutions corresponding to rather coarse meshes are shown in Fig. 2. It is seen that the pressure is

---

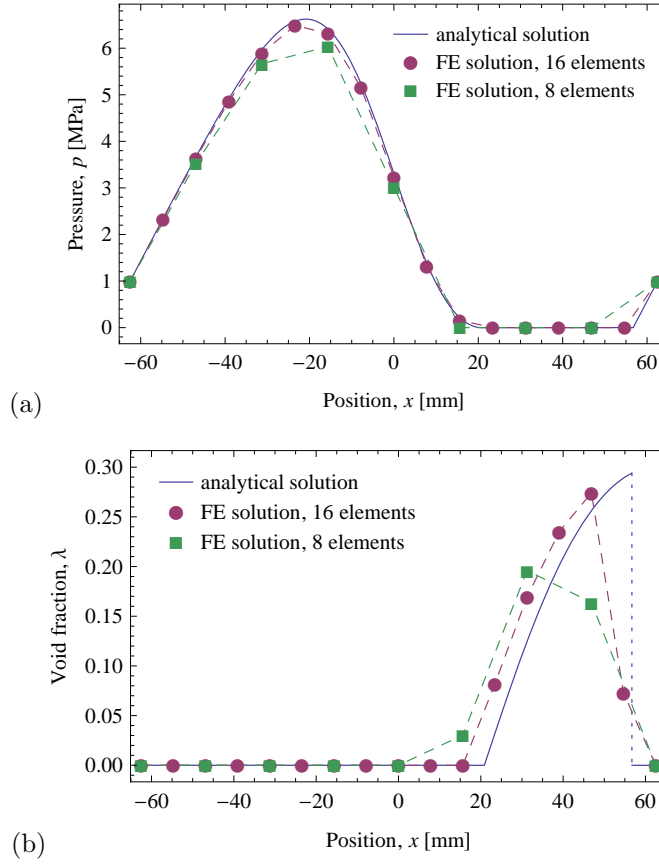[2]The code can also be downloaded from http://www.ippt.pan.pl/~sstupkie/files/bearing.nb.

Figure 2: Solution of the sinusoidal bearing problem: (a) pressure p, (b) void fraction λ. The dotted line indicates the jump of λ in the analytical solution.

reproduced fairly well using the mesh of just 16 elements. At the same time, the void fraction λ shows a more visible discrepancy with respect to the analytical solution. In particular, the analytical solution in λ exhibits a jump at the reformation boundary which can only be approximated by a continuous FE interpolation of λ.

Clearly, mesh refinement improves the accuracy. In particular, for finer meshes it is evident that the essential features of the analytical solution at the cavitation boundary (mentioned above) are properly represented by the FE solution. Convergence of the FE solution with mesh refinement is illustrated in Fig. 3 which shows the L_2 norm of the error in p and in λ evaluated at the nodes. The solution in p is second-order accurate, cf. Fig. 3a.

The error in λ is shown in Fig. 3b. The number of elements is varied

17

(a)

(b)
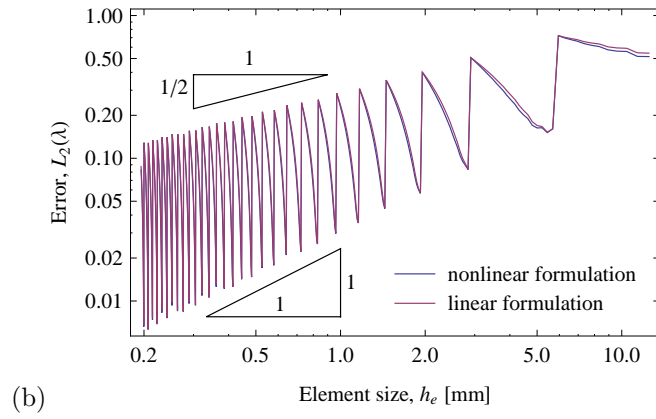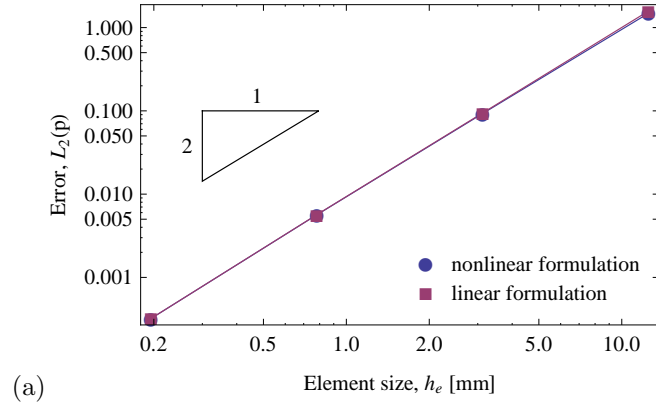
Figure 3: Convergence of the solution with mesh refinement for the sinusoidal bearing problem: L_2 norm of the error in (a) pressure p and (b) complementary variable λ.

18

between 10 and 640 with the step of 1, and it is seen that the error exhibits oscillations. This is related to the varying positioning of the nodes with respect to the exact position of the discontinuity of λ at the reformation boundary. The order of accuracy in λ is bounded between 1/2 and 1.

Note that the error in p in Fig. 3a is shown only for four mesh densities (10, 40, 160 and 640 elements), as indicated by the markers. When the error in p is evaluated at all intermediate mesh densities then some oscillations are also observed; however, their magnitude is much smaller than in the case of the error in λ.

In terms of accuracy, the difference between the nonlinear formulation (24) and linear formulation (30) is very small so that the corresponding lines are hardly distinguishable in Fig. 3. However, as expected, the error of the nonlinear formulation is always smaller than the error of the linear formulation. The difference decreases with increasing mesh density.

Finally, we note that, in case of the present problem, the number of iterations does not significantly increase with increasing mesh density, and it varies between 4 for coarse meshes and 8 for a very fine mesh of 32000 elements.

4.2. Sinusoidal bearing profile with sine-shaped fluctuations

The second example is a modification of the example of the previous subsection such that small-scale fluctuations of the film thickness are introduced with the period $l_2 = l/10$ and amplitude $\Delta h_2 = \Delta h/2$. The film thickness is thus now defined by

$$h(x) = h_{\mathrm{av}} - \Delta h \cos(2\pi x/l) - \Delta h_2 \cos(2\pi x/l_2), \tag{34}$$

see Fig. 4, and all the remaining parameters of the problem are specified in Section 4.1.

The solution obtained using a fine mesh of 1000 elements is shown in Fig. 5. It exhibits small-scale oscillations which are induced by the fluctuations of the film thickness. In particular, two cavitation regions are formed. As a result, the problem becomes more demanding for the computational scheme, as illustrated below.

Convergence of the solution with mesh refinement is assessed with respect to the numerical solution obtained using a very fine mesh of 10000 elements. Figure 6 shows the L_2 norm of the error in p as a function of element size. As in the previous example, the solution in p is second-order accurate. Also, the
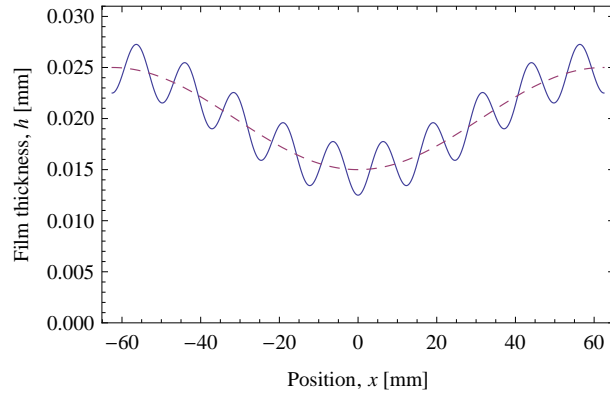
19

Figure 4: Sinusoidal bearing with sine-shaped fluctuations: film thickness h. The dashed line corresponds to the example of Section 4.1.
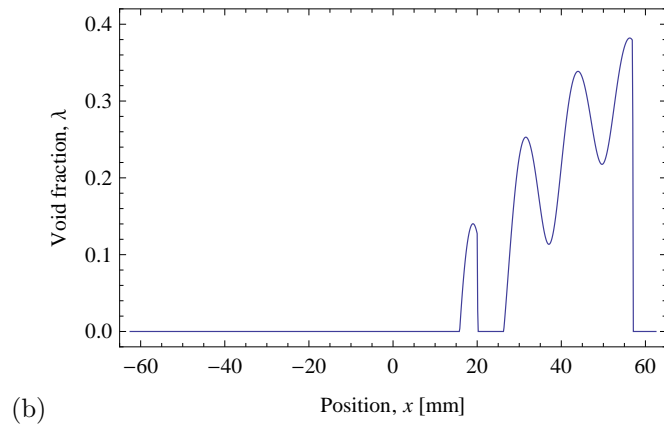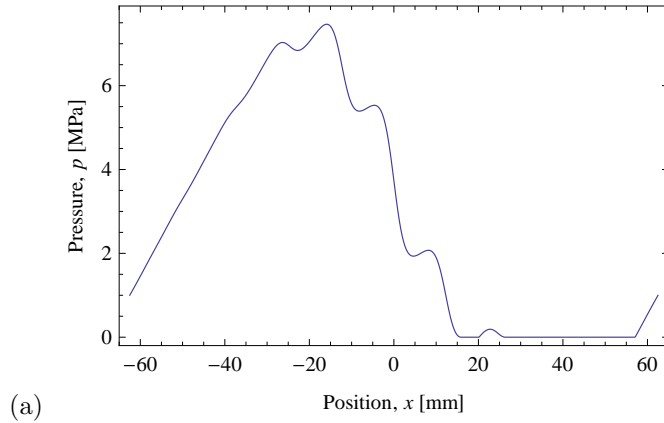

(a)

(b)

Figure 5: Sinusoidal bearing with sine-shaped fluctuations: (a) pressure p, (b) void fraction λ.
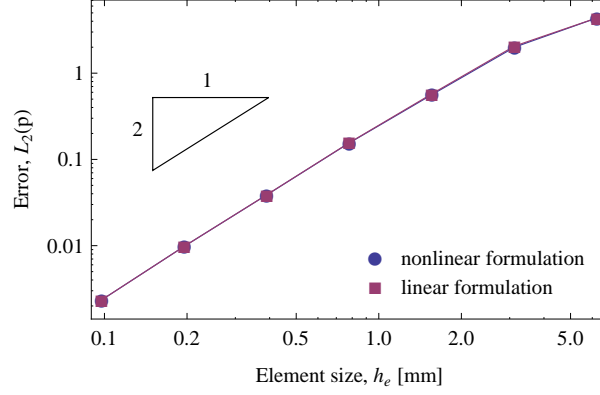
Figure 6: Convergence of the solution in pressure p with mesh refinement for the sinusoidal bearing with sine-shaped fluctuations.

accuracy of the linear and the nonlinear formulation is practically identical, the latter being slightly more accurate, particularly for coarser meshes.

The number of iterations is shown in Fig. 7. Unlike in the previous example, the number of iterations significantly increases with increasing mesh density reaching nearly 100 for the mesh of 6000 elements (note that, in the previous example, 8 iterations were sufficient for the mesh of 32000 elements). In terms of the number of iterations, the behaviour of the linear and the nonlinear formulation is similar. However, in case of the nonlinear formulation, the iterative scheme diverged for $N_e = 4000$, and the corresponding missing point is marked by an arrow in Fig. 7. This indicates that the linear formulation may be preferable due to its higher robustness.

4.3. Sinusoidal bearing profile in 2D

In this section, we study the example of Section 4.1 extended to two dimensions. The sinusoidal bearing profile is assumed constant along the y-direction,

$$h(x, y) = h_{av} - \Delta h \cos(2\pi x/l), \quad x \in (-l/2, l/2), \ y \in (-l/2, l/2), \quad (35)$$

and the 2D effects are introduced by prescribing a constant pressure on the whole boundary, $p(\pm l/2, y) = p(x, \pm l/2) = 1$ MPa.

The FE solution of this problem is shown in Fig. 8. The cavitation boundary has a zigzag appearance, and the solution in λ exhibits moderate oscil-
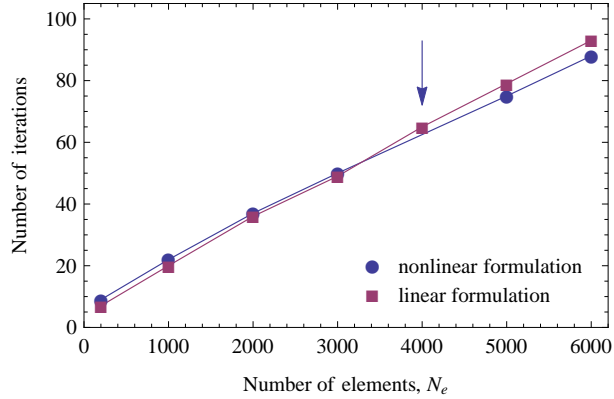
21

Figure 7: Number of iterations as a function the number of elements for the sinusoidal bearing with sine-shaped fluctuations.

lations along the curved part of the rupture boundary, see Fig. 8b. This, however, does not affect the solution in p, cf. Fig. 8a.

The results shown in Fig. 8a,b have been obtained using the standard Gaussian quadrature applied to the mass-balance equation (24). Interestingly, when the nodal (Lobatto) quadrature is used instead, an oscillation-free solution is obtained, as shown in Fig. 8c.

Convergence of the solution with mesh refinement is assessed with respect to the numerical solution obtained using a fine mesh of $640{\times}640$ elements. Figure 9 shows the L_2 norm of the error in p as a function of element size for the linear and the nonlinear formulation and for the Gaussian and the nodal quadrature. Again, the solution in p is approximately second-order accurate, and the accuracy of the linear and the nonlinear formulation is very similar, provided the latter converges to a correct solution. The arrow in Fig. 9 indicates the finest mesh for which a correct converged solution was obtained for the nonlinear formulation. Figure 9 also shows that the nodal quadrature is less accurate than the Gaussian quadrature, despite the latter leads to spurious oscillations in λ. Those oscillations persist when the mesh is refined so that the error in λ is slightly higher for the Gaussian quadrature (the corresponding results are not included here for brevity).

Figure 10 shows the number of iterations which, in case of the linear formulation and Gaussian quadrature, reaches 32 for a regular mesh of $500{\times}500$ elements. As mentioned above, the nonlinear formulation exhibits convergence problems for both quadrature rules, and the arrow in Fig. 10 indicates
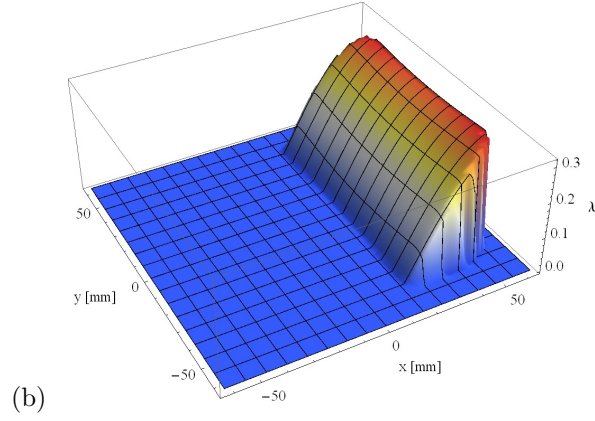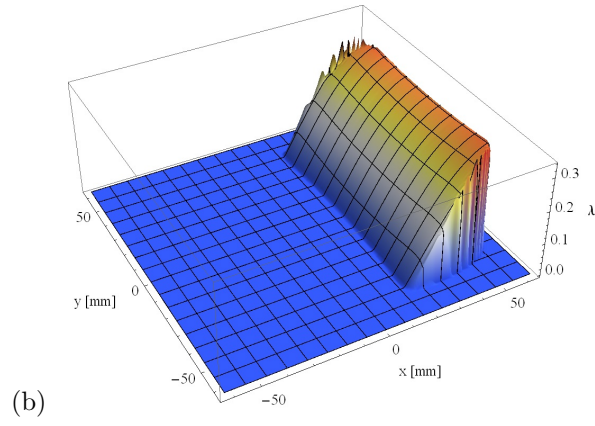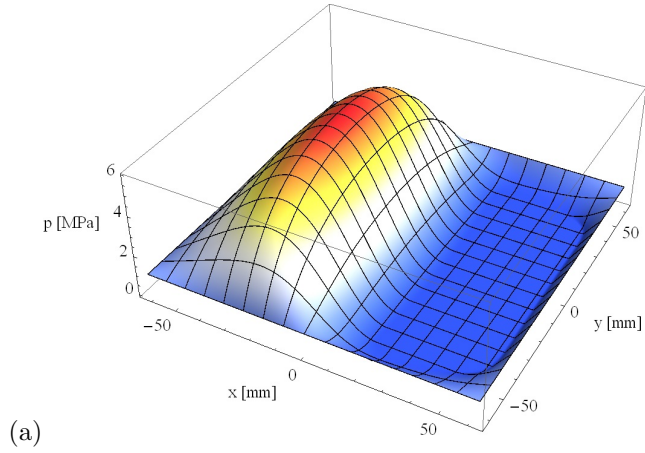
22

(a)

(b)

(b)

Figure 8: Sinusoidal bearing in 2D: (a) pressure p (Gaussian quadrature), (b) void fraction λ (Gaussian quadrature), (c) void fraction λ (Lobatto quadrature). The grid is included for visualization purposes; the solution has been obtained using a much finer mesh of 160×160 elements.
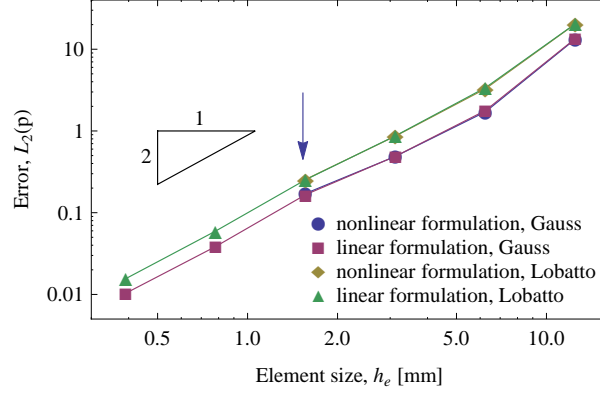
Figure 9: Convergence of the solution in pressure p with mesh refinement for the sinusoidal bearing in 2D.

the finest mesh for which the iterative scheme converged to a correct solution. The Gaussian quadrature appears less efficient which is probably related to the oscillations in λ.

4.4. Oscillatory squeeze flow

In this section, solution of a one-dimensional problem of oscillatory squeeze flow is presented in order to illustrate applicability of the method to transient lubrication problems. The respective formulation is presented in Appendix B. The example and its parameters are taken from [7]; similar problems have also been studied, for instance, in [38, 39, 23].

Consider a one-dimensional pure squeeze flow between two parallel rigid plates. The problem is defined by specifying the thickness of the fluid film,

$$\bar{h}(\bar{t}) = 0.125 \cos(4\pi\bar{t}) + 0.375, \tag{36}$$

and the boundary conditions for pressure $\bar{p} = \bar{p}(\bar{x}, \bar{t})$,

$$\bar{p}(0, \bar{t}) = \bar{p}(1, \bar{t}) = 0.025, \tag{37}$$

while the entrainment speed is assumed equal to zero. All the quantities are here dimensionless with h^*, t^* and x^* denoting the characteristic film thickness, time and length, respectively, so that $\bar{h} = h/h^*$, $\bar{t} = t/t^*$, and $\bar{x} = x/x^*$, while the pressure $\bar{p} = p/p^*$ is normalized using $p^* = (6\eta/t^*)(x^*/h^*)^2$.
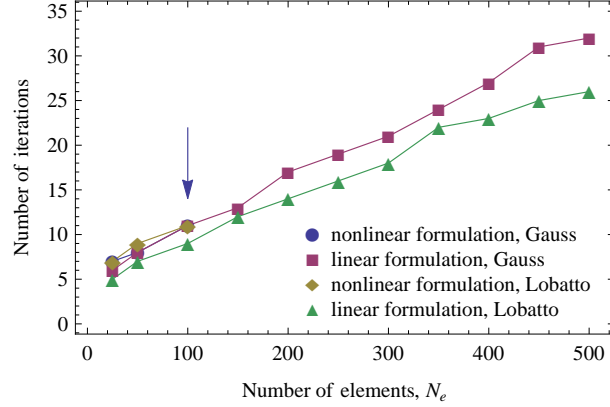
24

Figure 10: Number of iterations as a function the number N_e of elements for the sinusoidal bearing in 2D. N_e denotes here the number of elements along each direction (x and y), the total number of elements in N_e^2.

Ausas et al. [7] presented an analytical solution to this problem. Shortly after $\bar{t} \approx 0.25$, a cavitation zone nucleates in the center of the domain. Subsequently, the cavitation zone expands and then it shrinks until it disappears shortly before $\bar{t} = 0.75$. This process is repeated in a cyclic manner with the period $\bar{T} = 0.5$. The cavitation zone is symmetric with respect to $\bar{x} = 0.5$.

Figure 11 shows the dimensionless position of the right cavitation boundary as a function of time (the first two cycles are shown). The finite element solution is compared to the analytical solution of [7]. The FE solution has been obtained using 100 elements and time increment $\Delta \bar{t} = 0.01$. The agreement is very good, and it has been checked that the agreement is further improved with mesh refinement.

The FE discretization results in stepwise changes of the position of the cavitation boundary which is clearly visible in Fig. 11(b). Figure 11(b) also shows the effect of the $(1 - \lambda)$ term in the Poiseuille term in the nonlinear formulation. In agreement with the results reported previously, the nonlinear formulation is slightly more accurate than the linear one. At the same time, the number of iterations is somewhat higher in case of the nonlinear formulation, again in agreement with the previous results. This is illustrated in Fig. 12. It is seen that the iterative scheme converges in 2–4 iterations except in the vicinity of the time instants at which the cavitation zone nucleates or vanishes. At those time instants, the number of iterations exceeds 15. It has been checked that this number further increases with increasing
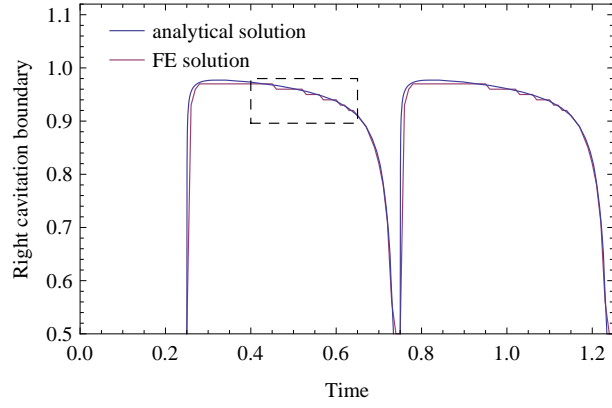
(a)
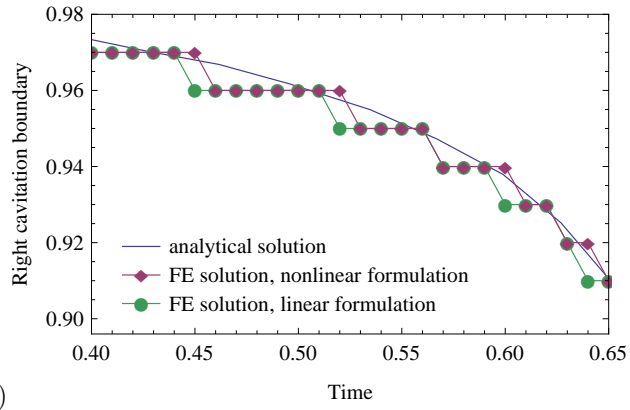
(b)

Figure 11: Oscillatory squeeze flow: (a) position of the right cavitation boundary during first two cycles, (b) detailed view of the region marked by the dashed line in figure (a). The FE solution is compared to the analytical solution provided in [7].
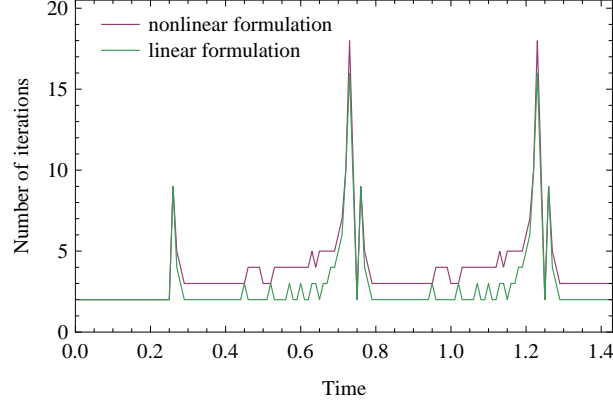
26

Figure 12: Number of iterations as a function of time for the oscillatory squeeze flow problem.

mesh density (the corresponding results are not provided here).

4.5. 3D soft-EHL problem: hyperelastic ball

The last example illustrates the application of the present cavitation model to a fully coupled soft-EHL problem. The adopted finite-deformation formulation and its FE implementation are outlined in Section 3.3.

A hyperelastic ball of radius $R = 9.25$ mm is sliding against a rigid plane at a constant sliding velocity U along the x-axis so that we have $u = U/2$. A steady-state lubrication problem is analyzed in a reference frame attached to the ball, and the problem is solved for several values of the entrainment speed u varying between 20 and 800 mm/s. A constant normal force $F = 13$ N is applied at the mid-plane of the ball by constraining all the displacements at the mid-plane and by adjusting the vertical displacement such that the normal force is constant. The cavitation pressure is assumed equal to zero, $p_{\mathrm{cav}} = 0$, and the boundary condition $p = 0$ is prescribed far from the actual contact zone, thus fully flooded conditions are assumed. The hyperelastic behaviour of the ball is governed by a nearly incompressible neo-Hookean model with the Young's modulus $E = 2.4$ MPa, and the Poisson's ratio $\nu = 0.49$. A constant lubricant viscosity is assumed with $\eta = 0.78$ Pa s. These parameters correspond to a PDMS ball and glycerol (96 wt %)/water solution, cf. [40].

The finite element mesh is shown in Fig. 13a. Note that symmetry is exploited in order to reduce the number of unknowns. In agreement with the
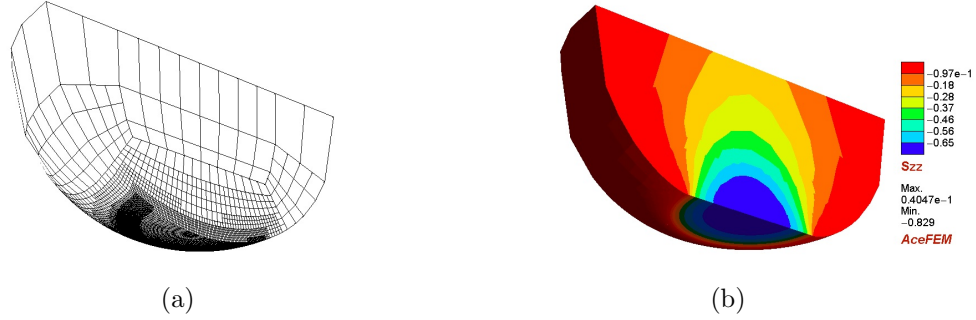
27

Figure 13: Hyperelastic ball: (a) finite element mesh in the undeformed configuration, (b) σ_{zz} component of the Cauchy stress tensor in the deformed configuration.

2D results reported in [26], a very fine mesh is needed to avoid oscillations in more severe lubrication conditions, i.e., when the film thickness is relatively small. The mesh is thus significantly refined in the zones of high pressure gradients, as can be seen in Fig. 13a.

Figure 13b shows the σ_{zz} component of the Cauchy stress tensor in the deformed configuration. Finite deformation of the ball is clearly visible in Fig. 13b. At the contact force of 13 N, the radius of the contact zone is about 3.75 mm (i.e., about 40% the initial ball radius), and the maximum contact pressure is 0.83 MPa (i.e., about 35% of the initial Young's modulus).

The details of the solution in the lubricated contact zone are illustrated in Fig. 14. The map of film thickness h in Fig. 14c shows a characteristic ridge that forms along the trailing edge of the contact zone with the minimum film thickness at the ends of the ridge, in a qualitative agreement with many experimental and numerical results, e.g., [41]. The film-thickness profiles corresponding to different entrainment speeds are shown in Fig. 15. The width of the ridge decreases with decreasing entrainment speed, and for $u = 20$ mm/s it spans only 3-4 elements. Simulation of the present soft-EHL problem at lower values of u would thus require further refinement of the finite element mesh. Small oscillations of the film thickness are visible at the locations of abrupt change of element size. Figure 16 shows the pressure profiles along the symmetry axis corresponding to $u = 20$ mm/s and $u = 800$ mm/s. Note that the markers in Fig. 16 are included for every 20th node, i.e., the actual mesh used in the computations is 20 times finer than suggested by the markers.

The friction coefficient is shown in Fig. 17 as a function of the entrainment
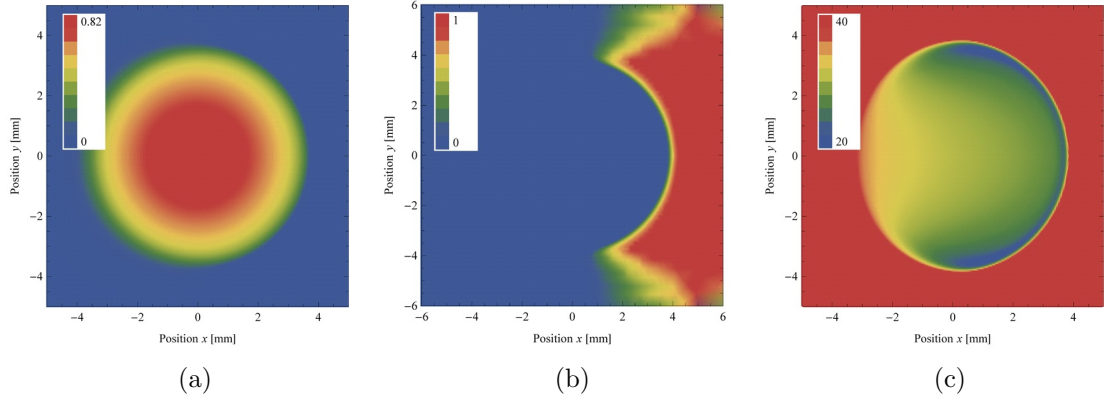
Figure 14: Maps of (a) pressure p (in MPa), (b) void fraction λ, and (c) film thickness h (in μm) obtained for $u = 400$ mm/s.

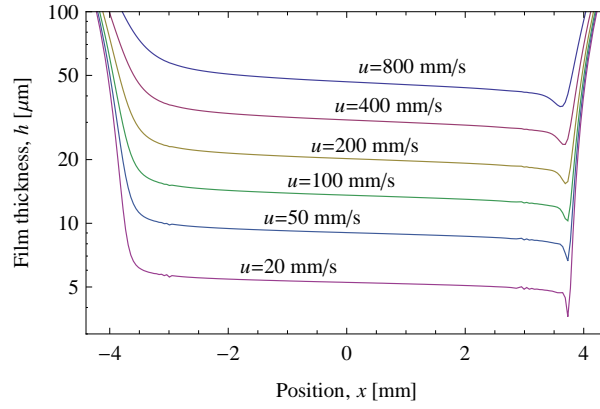

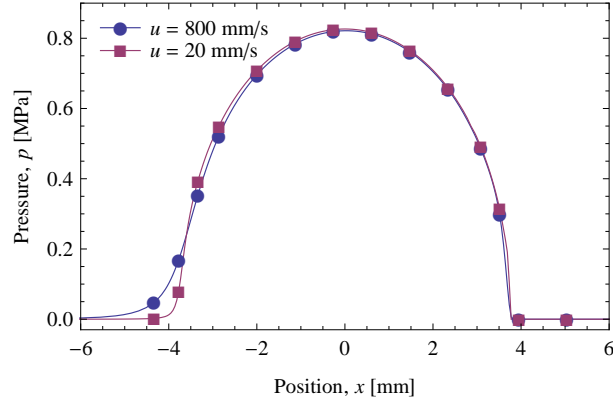Figure 15: Film-thickness profiles in the symmetry plane $y = 0$.

Figure 16: Pressure profiles in the symmetry plane $y = 0$. The markers indicate every 20th node of the FE mesh.
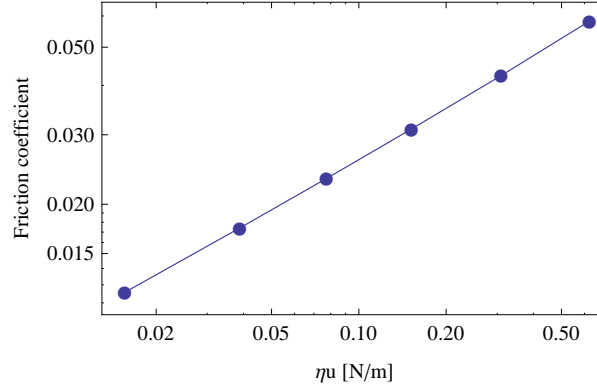
Figure 17: Friction coefficient as a function of the entrainment speed u.

speed u. The dependence is approximately linear on a log–log scale which is typical for the EHL regime. Finite deformations seem not to affect this linearity, at least in the range of process parameters studied in this work. It is recalled that the effect of the friction forces on the ball deformation is fully accounted for in the present model.

5. Conclusion

The paper is concerned with the formulation and finite-element implementation of a mass-conserving cavitation model. A mixed formulation has been introduced in which the hydrodynamic pressure p and the complemen-

tary variable λ related to lubricant density are treated as independent variables. The complementarity of the two variables is then enforced using a non-smooth constraint function, and the discretized problem is solved simultaneously for both variables using the semi-smooth Newton method. The approach is directly applicable to fully coupled soft-EHL problems, as illustrated by a numerical example involving finite deformations. The monolithic Newton-based solution scheme proved highly efficient for the soft-EHL problem considered.

The weak form of the mass-balance equation has been derived as a basis of the finite element discretization. Here, some details of the formulation have been indicated which seemingly have not been noticed so far. Their impact on the performance of the computational scheme has been found not much pronounced. Specifically, upon neglecting an inessential nonlinear term in the weak form, the rigid-isoviscous lubrication problem becomes a linear complementarity problem [22]. The full nonlinear formulation has been found slightly more accurate than the linear one, but it typically requires more iterations. More importantly, it is less stable in the sense that in some cases the corresponding iterative scheme does not converge or it converges to a non-physical solution. The reported results suggest thus that the linear formulation is preferable due to its higher robustness while the associated loss in accuracy is in practice negligible.

By exploiting the complementarity conditions, the proposed (two-field) mixed formulation can be transformed to the single-field formulation of [12]. Whenever applicable, the latter is preferable, as the number of unknowns of the cavitation model is reduced by the factor of two. Some situations in which the two-field formulation is preferable are discussed in Appendix C. In particular, the present finite-element treatment of the fully coupled soft-EHL problem relies on the two-field formulation, which is due to the specific mesh refinement technique adopted. Note that, in the case of the soft-EHL problem, the additional cost of introducing an extra scalar variable on the lubricated boundary is negligible because the nodal displacements in the solid constitute the vast majority of the global unknowns.

Appendix A. Derivation of the weak form

This appendix details the derivation of the weak form (13) starting from Eq. (11). We remind that integration by parts is applied only to the Poiseuille term. As the pressure gradient suffers discontinuity at the reformation bound-

ary, the integral over Ω in Eq. (11) is first split into two integrals over Ω_{f} and Ω_{c}

$$\int_{\Omega_{\mathrm{f}}} \delta p \, \nabla \cdot \left(\varrho \boldsymbol{u} h - \frac{\varrho h^3}{12\eta} \nabla p \right) \mathrm{d}\Omega + \int_{\Omega_{\mathrm{c}}} \delta p \, \nabla \cdot (\varrho \boldsymbol{u} h) \, \mathrm{d}\Omega = 0, \qquad (\text{A.1})$$

where the corresponding definitions (2) and (5) of $\boldsymbol{q}$ have been used. Integration by parts is then applied in Ω_{f} to the term involving pressure gradient in order to reduce the order of differentiation,

$$\int_{\Omega_{\mathrm{f}}} \nabla \delta p \cdot \left(\frac{\varrho h^3}{12\eta} \nabla p \right) \mathrm{d}\Omega - \int_{\partial\Omega_{\mathrm{f}}} \delta p \, \frac{\varrho h^3}{12\eta} \nabla p \cdot \boldsymbol{n} \, \mathrm{d}\Gamma$$

$$+ \int_{\Omega_{\mathrm{f}}} \delta p \, \nabla \cdot (\varrho \boldsymbol{u} h) \, \mathrm{d}\Omega + \int_{\Omega_{\mathrm{c}}} \delta p \, \nabla \cdot (\varrho \boldsymbol{u} h) \, \mathrm{d}\Omega = 0, \qquad (\text{A.2})$$

where $\boldsymbol{n}$ is the unit outward normal to Ω_{f}. The second integral vanishes on $\partial\Omega_{\mathrm{f}} \cap \partial\Omega$ in view of Eq. (12), so that only the integral over the cavitation boundary Σ remains with $\boldsymbol{n} = -\boldsymbol{\nu}$,

$$\int_{\Omega_{\mathrm{f}}} \nabla \delta p \cdot \left(\frac{\varrho h^3}{12\eta} \nabla p \right) \mathrm{d}\Omega + \int_{\Omega} \delta p \, \nabla \cdot (\varrho \boldsymbol{u} h) \, \mathrm{d}\Omega$$

$$+ \int_{\Sigma} \delta p \left(\frac{\varrho h^3}{12\eta} \nabla p \right)^{+} \cdot \boldsymbol{\nu} \, \mathrm{d}\Gamma = 0, \qquad (\text{A.3})$$

where the superscript $+$ indicates that the pressure gradient is taken at the full-film side of the cavitation boundary. Noting that $\nabla p = \boldsymbol{0}$ in Ω_{c}, the first integral in Eq. (A.3) can be equivalently performed on the whole domain Ω, thus

$$\int_{\Omega} \left[\nabla \delta p \cdot \left(\frac{\varrho h^3}{12\eta} \nabla p \right) + \delta p \, \nabla \cdot (\varrho \boldsymbol{u} h) \right] \mathrm{d}\Omega + \int_{\Sigma} \delta p \left(\frac{\varrho h^3}{12\eta} \nabla p \right)^{+} \cdot \boldsymbol{\nu} \, \mathrm{d}\Gamma = 0. \tag{A.4}$$

Finally, considering the mass-flux continuity condition (6) with $\boldsymbol{q}^{+}$ and $\boldsymbol{q}^{-}$ defined by Eqs. (2) and (5), respectively, the integral over the on the cavitation boundary Σ is transformed to

$$\int_{\Omega} \left[\nabla \delta p \cdot \left(\frac{\varrho h^3}{12\eta} \nabla p \right) + \delta p \, \nabla \cdot (\varrho \boldsymbol{u} h) \right] \mathrm{d}\Omega + \int_{\Sigma} \delta p (\varrho^{+} - \varrho^{-}) h \boldsymbol{u} \cdot \boldsymbol{\nu} \, \mathrm{d}\Gamma = 0, \tag{A.5}$$

which now involves the jump of density ϱ rather than the jump of the pressure gradient. The weak form (13) is obtained by introducing the relative density $\bar{\varrho} = \varrho / \varrho_0$.

Appendix B. Transient lubrication problem

In this section, we outline the extension of the present finite element formulation to transient lubrication problems. The details are omitted, and only the resulting mass-balance equation in weak form is provided.

In the continuum formulation of a transient lubrication problem, the mass balance equation (1) is replaced by

$$\nabla \cdot (\varrho \boldsymbol{q}) + \frac{\partial(\varrho h)}{\partial t} = 0 \quad \text{in } \Omega, \tag{B.1}$$

the formulae (2)–(5) for the flux $\boldsymbol{q}$ remain unaltered, while the continuity condition (6) is supplemented by additional terms due to discontinuity of density and propagation of the cavitation boundary Σ.

Detailed derivation of the weak form of the mass-balance equation is not attempted here, as it is somewhat more involved than the procedure presented above for the case of the steady-state problems. However, the final result can be obtained in a straightforward manner by observing that the actual finite element formulation relies on a *continuous* approximation of λ and by exploiting this continuity. The result is that the time derivative of $(1-\lambda^h)h$ is simply added to the weak form (24) as a source term. The implicit backward-Euler method is then applied to approximate the time derivative which finally yields

$$\int_{\Omega^h} \left[\nabla \delta p^h \cdot \left(\frac{(1 - \lambda^h) h^3}{12\eta} \nabla p^h \right) + \delta p^h \, \nabla \cdot (\boldsymbol{u} h) \right.$$
$$\left. - \delta \tilde{p}^h \, \nabla \cdot (\lambda^h \boldsymbol{u} h) + \delta p^h \, \frac{(1 - \lambda^h) h - (1 - \lambda_n^h) h_n}{\Delta t} \right] \mathrm{d}\Omega \;\; = \;\; 0. \tag{B.2}$$

Here, λ_n^h and h_n refer to the previous time step t_n, while all the quantities without the subscript refer to the current time step $t_{n+1} = t_n + \Delta t$. The problem is solved at t_{n+1}, and the computational scheme proceeds in an incremental manner.

The above formulation has been applied to solve the oscillatory squeeze flow problem. The results are presented in Section 4.4.

Appendix C. Single-field formulation

As described in Section 3.1, the nodal quadrature is applied to Eq. (25) so that the complementarity conditions are enforced at the nodes. It can

be easily checked that upon application of the iterative scheme (29) we have at each node either $p_i^{k+1} = 0$ or $\lambda_i^{k+1} = 0$, regardless of the previous values p_i^k and λ_i^k. The complementarity conditions can thus be used to reduce the number of actual unknowns by introducing a single variable D such that $D > 0$ corresponds to the pressure p (with $\lambda = 0$) and $D < 0$ corresponds to $-\lambda$ (with $p = 0$), cf. [12]. Similar treatments can be found in [8, 9]. The lubrication and cavitation problem is then governed by a single equation

$$
\int_{\Omega^h} \left[\nabla \delta D^h \cdot \left(\frac{(1 - \lambda^h) h^3}{12\eta} \, \nabla p^h \right) + \delta D^h \, \nabla \cdot (\boldsymbol{u} h) - \delta \tilde{D}^h \, \nabla \cdot (\lambda^h \boldsymbol{u} h) \right] \mathrm{d}\Omega = 0,
\tag{C.1}
$$

where

$$
D^h = \sum_i N_i D_i, \qquad \delta D^h = \sum_i N_i \delta D_i,
\tag{C.2}
$$

while p^h and λ^h are now defined by Eq. (21) with the nodal quantities p_i and λ_i defined in terms of the nodal unknowns D_i according to

$$
p_i = \begin{cases} D_i & \text{if } D_i \geq 0, \\ 0 & \text{otherwise,} \end{cases} \qquad \lambda_i = \begin{cases} 0 & \text{if } D_i \geq 0, \\ -D_i & \text{otherwise.} \end{cases}
\tag{C.3}
$$

This above single-field formulation is the basis of the computational model developed in [12] for transient lubrication problems. The notation adopted above is somewhat different from that in [12], but the two formulations are fully equivalent.

The obvious benefit of the single-field formulation is the reduction of the number of unknowns by the factor of two. However, the two-field mixed formulation of Section 3.1 is more general and more flexible, and there are some situations in which it may be preferable to the single-field formulation, as discussed below. Otherwise, the above single-field formulation and the two-field formulation proposed in this work are equivalent, including the convergence behaviour of the iterative scheme (29).

Enforcement of the complementarity conditions at the nodes is a crucial element of the single-field formulation. At the same time, numerical quadrature of (20) with integration points at the nodes is just one option that has been found effective and has been followed in this work, but alternative approaches can possibly be developed starting from the present two-field formulation.

One may also consider a refined iterative solution scheme replacing that defined in Eq. (29). For instance, a line search technique may be employed

instead of the full Newton step in Eq. (29). Then, the complementarity condition would not necessarily be satisfied after each iteration, and the single- and two-field formulations would no longer be fully equivalent. In case of the two-field formulation, one might also supply to the iterative scheme (29) an initial guess $(\mathbf{p}^0, \boldsymbol{\lambda}^0)$ that does not satisfy the complementarity condition.

Further, the flexibility of the two-field formulation appears beneficial when mesh refinement is used. In particular, implementation of the mesh refinement technique using so-called hanging-nodes is straightforward in case of the two-field formulation, while the single-field formulation would require special treatment of both complementary variables at the hanging nodes. Note that mesh refinement using the hanging-node technique has been a crucial element of the soft-EHL example of Section 4.5.

Finally, when a fully coupled EHL problem is solved and the solid deformation subproblem is nonlinear, e.g., due to the finite deformation effects, as in the soft-EHL example of Section 4.5, the deformation of the solid is typically modelled using the finite element method. Then, the unknowns corresponding to the hydrodynamic pressure p constitute only a small fraction of all unknowns, and the extra computational cost due to additional unknowns corresponding to the complementary variable λ is not significant. For instance, in the soft-EHL problem of Section 4.5, the total number of unknowns is about 295000 of which only $2 \times 10800 = 21600$ correspond to the hydrodynamic pressure p and the complementary variable λ.

[1] B. Jakobsson, L. Floberg, The finite journal bearing considering vaporization, Transactions of Chalmers University Technology, vol. 190, Goteborg, Sweden, 1957.

[2] K. O. Olsson, Cavitation in dynamically loaded bearings, Transactions of Chalmers University Technology, vol. 308, Goteborg, Sweden, 1965.

[3] H. G. Elrod, M. L. Adams, A computer program for cavitation and starvation problems, in: D. Dowson, M. Godet, C. M. Taylor (Eds.), Proc. of the First Leeds–Lyon Symposium on Tribology – Cavitation

and Related Phenomena in Lubrication, Mechanical Engineering, New York, 1974, pp. 37–41.

[4] H. G. Elrod, A cavitation algorithm, Trans. ASME J. Lubr. Technol. 103 (1981) 350–354.

[5] D. Vijayaraghavan, T. G. Keith, Development and evaluation of a cavitation algorithm, Tribol. Trans. 32 (1989) 225–233.

[6] R. S. Paranjpe, P. K. Goenka, Analysis of crankshaft bearings using a mass conserving algorithm, Tribol. Trans. 33 (1990) 333–344.

[7] R. F. Ausas, M. Jai, G. C. Buscaglia, A mass-conserving algorithm for dynamical lubrication problems with cavitation, Trans. ASME J. Tribol. 131 (2009) 031702.

[8] G. Bayada, M. Chambat, M. El Alaoui, Variational formulations and finite element algorithms for cavitation problems, Trans. ASME J. Tribol. 112 (1990) 398–403.

[9] A. Kumar, J. F. Booker, A finite element cavitation algorithm, Trans. ASME J. Tribol. 113 (1991) 276–284.

[10] D. Bonneau, D. Guines, J. Frene, J. Topolsky, EHD analysis, including structural inertia effects and a mass-conserving cavitation model, Trans. ASME J. Tribol. 117 (1995) 540–547.

[11] G. Bayada, M. Chambat, A finite element algorithm for cavitation in hydrodynamic lubrication, Rev. Eur. Elem. Finis 10 (2001) 653–678.

[12] M. Hajjam, D. Bonneau, A transient finite element cavitation algorithm with application to radial lip seals, Tribol. Int. 40 (2007) 1258–1269.

[13] G. Bayada, M. Chambat, C. Vazquez, Characteristics method for the formulation and computation of a free boundary cavitation problem, J. Comp. Appl. Math. 98 (1998) 191–212.

[14] S. J. Alvarez, R. Oujja, An iterative method for solving a free boundary problem for an infinite journal bearing, Appl. Math. Comp. 122 (2001) 15–26.

[15] M. J. Braun, W. M. Hannon, Cavitation formation and modelling for fluid film bearings: a review, Proc. Instn. Mech. Engrs. Part J: J. Engng. Tribol. 224 (2010) 839–863.

[16] F. P. Grando, M. Priest, A. T. Prata, A two-phase flow approach to cavitation modelling in journal bearings, Tribol. Lett. 21 (2006) 233–244.

[17] T. Geike, V. Popov, Cavitation within the framework of reduced description of mixed lubrication, Tribol. Int. 42 (2009) 93–98.

[18] G. Bayada, L. Chupin, Compressible fluid model for hydrodynamic lubrication cavitation, Trans. ASME J. Tribol. 135 (2013) 041702–1–13.

[19] M. M. Kostreva, Elasto-hydrodynamic lubrication: a non-linear complementarity problem, Int. J. Num. Meth. Fluids 4 (1984) 377–397.

[20] K. P. Oh, The numerical solution of dynamically loaded elastohydrodynamic contact as a nonlinear complementarity problem, Trans. ASME J. Tribol. 106 (1984) 88–95.

[21] A. Strozzi, Formulation of three lubrication problems in terms of complementarity, Wear 104 (1985) 103–119.

[22] M. Giacopini, M. T. Fowell, D. Dini, A. Strozzi, A mass-conserving complementarity formulation to study lubricant films in the presence of cavitation, Trans. ASME J. Tribol. 132 (2010) 041702–1–12.

[23] L. Bertocchi, D. Dini, M. Giacopini, M. T. Fowell, A. Baldini, Fluid film lubrication in the presence of cavitation: a mass-conserving two-dimensional formulation for compressible, piezoviscous and non-Newtonian fluids, Tribol. Int. 67 (2013) 61–71.

[24] J. de Vicente, J. R. Stokes, H. A. Spikes, The frictional properties of Newtonian fluids in rolling–sliding soft-EHL contact, Tribol. Lett. 20 (2005) 273–286.

[25] S. Stupkiewicz, A. Marciniszyn, Elastohydrodynamic lubrication and finite configuration changes in reciprocating elastomeric seals, Tribol. Int. 42 (2009) 615–627.

[26] S. Stupkiewicz, Finite element treatment of soft elastohydrodynamic lubrication problems in the finite deformation regime, Comp. Mech. 44 (2009) 605–619.

[27] O. C. Zienkiewicz, R. L. Taylor, The Finite Element Method. Volume 1: The Basics, Butterworth-Heinemann, Oxford, 5th edition, 2000.

[28] M. El Alaoui Talibi, M. Jai, Existence and numerical results of a transient lubrication problem with cavitation, J. Math. Anal. Appl. 394 (2012) 260–275.

[29] D. P. Bertsekas, Constrained Optimization and Lagrange Multiplier Methods, Athena Scientific, Belmont, MA, 2nd edition, 1996.

[30] M. Hintermueller, K. Ito, K. Kunisch, The primal-dual active set strategy as a semismooth Newton method, SIAM J. Optim. 13 (2003) 865–888.

[31] P. Alart, A. Curnier, A mixed formulation for frictional contact problems prone to Newton like solution methods, Comp. Meth. Appl. Mech. Engng. 92 (1991) 353–375.

[32] S. Hueber, B. Wohlmuth, A primal–dual active set strategy for nonlinear multibody contact problems, Comp. Meth. Appl. Mech. Engng. 194 (2005) 3147–3166.

[33] J. Korelc, Automation of primal and sensitivity analysis of transient coupled problems, Comp. Mech. 44 (2009) 631–649.

[34] T. J. R. Hughes, A. N. Brooks, A multidimensional upwind scheme with no crosswind diffusion, in: T. J. R. Hughes (Ed.), Finite Elements for Convection Dominated Problems, volume 34 of *AMD*, ASME, New York, 1979.

[35] A. N. Brooks, T. J. R. Hughes, Streamline upwind/Petrov–Galerkin formulations for convection dominated flows with particular emphasis on the incompressible Navier–Stokes equations, Comp. Meth. Appl. Mech. Engng. 32 (1982) 199–259.

[36] O. C. Zienkiewicz, R. L. Taylor, The Finite Element Method, Butterworth-Heinemann, Oxford, 5th edition, 2000.

[37] E. A. de Souza Neto, D. Perić, M. Dutko, D. R. J. Owen, Design of simple low order finite elements for large strain analysis of nearly incompressible solids, Int. J. Sol. Struct. 33 (1996) 3277–3296.

[38] S. Boedo, J. F. Booker, Cavitation in normal separation of square and circular plates, Trans. ASME J. Tribol. 117 (1995) 403–410.

[39] V. Optasanu, D. Bonneau, Finite element mass-conserving cavitation algorithm in pure squeeze motion. Validation/application to a conneting-rod small end bearing, Trans. ASME J. Tribol. 122 (2000) 162–169.

[40] J. H. H. Bongaerts, J. P. R. Day, C. Marriott, P. D. A. Pudney, A. M. Williamson, In situ confocal Raman spectroscopy of lubricants in a soft elastohydrodynamic tribological contact, J. Appl. Phys. 104 (2008) 014913.

[41] L. Mourier, D. Mazuyer, A. A. Lubrecht, C. Donnet, Transient increase of film thickness in micro-textured EHL contacts, Tribol. Int. 39 (2006) 1745–1756.